

5-9-2017

Discontinuities in the electromagnetic fields of vortex beams in the complex source-sink model

Andrew Vikartofsky

University of Nebraska - Lincoln, avikartofsky2@unl.edu

Liang-Wen Pi

University of Nebraska-Lincoln, lpi@unl.edu

Anthony F. Starace

University of Nebraska-Lincoln, astarace1@unl.edu

Follow this and additional works at: <http://digitalcommons.unl.edu/physicsstarace>

 Part of the [Atomic, Molecular and Optical Physics Commons](#), [Elementary Particles and Fields and String Theory Commons](#), and the [Plasma and Beam Physics Commons](#)

Vikartofsky, Andrew; Pi, Liang-Wen; and Starace, Anthony F., "Discontinuities in the electromagnetic fields of vortex beams in the complex source-sink model" (2017). *Anthony F. Starace Publications*. 221.
<http://digitalcommons.unl.edu/physicsstarace/221>

This Article is brought to you for free and open access by the Research Papers in Physics and Astronomy at DigitalCommons@University of Nebraska - Lincoln. It has been accepted for inclusion in Anthony F. Starace Publications by an authorized administrator of DigitalCommons@University of Nebraska - Lincoln.

Discontinuities in the electromagnetic fields of vortex beams in the complex source-sink model

Andrew Vikartofsky, Liang-Wen Pi, and Anthony F. Starace

Department of Physics and Astronomy, The University of Nebraska, Lincoln, Nebraska 68588-0299, USA

(Received 7 March 2017; published 9 May 2017)

An analytical discontinuity is reported in what was thought to be the discontinuity-free exact nonparaxial vortex beam phasor obtained within the complex source-sink model. This discontinuity appears for all odd values of the orbital angular momentum mode. Such discontinuities in the phasor lead to nonphysical discontinuities in the real electromagnetic field components. We identify the source of the discontinuities, and provide graphical evidence of the discontinuous real electric fields for the first and third orbital angular momentum modes. A simple means of avoiding these discontinuities is presented.

DOI: [10.1103/PhysRevA.95.053826](https://doi.org/10.1103/PhysRevA.95.053826)**I. INTRODUCTION**

The worldwide effort to develop increasingly powerful lasers will allow the exploration of new physical regimes of intense laser interactions with matter as well as the development of new applications that such intense laser regimes permit [1,2]. Experimentally, the highest laser intensities are obtained using tight focusing techniques, in which the laser spot size in the focal region is comparable to the laser field wavelength. Theoretical simulations of laser-matter interactions under such tight focusing conditions require a detailed description of the laser fields in the focal region that goes beyond the paraxial approximation [3–9].

Laser beams that carry orbital angular momentum (OAM) provide another means of investigation into laser-matter interactions [10–12]. Consideration of light with nonzero OAM has been increasing in many fields including harmonic generation [13–15], particle acceleration [16,17], and quantum information [18,19]. Multiple nonparaxial analytic representations [20–23] have been developed to model tightly focused beams with nonzero OAM. One particularly important representation for a free space beam is the Laguerre-Gaussian (LG) basis, which can be used to represent optical vortices of any angular momentum mode [24].

The *complex point-source* model [25–27] is one tool that has been developed to analytically describe focused beams carrying OAM. This model is used to find solutions to the nonparaxial Helmholtz equation. This model assumes that the beam source exists at a complex point whose real value lies along the beam’s axis, and that the beam can be represented by an outgoing spherical wave. It was shown by Couture and Belanger [28] that (for an appropriate choice of boundary conditions) the spherical waves represented by this model are equivalent to the paraxial representation of a Gaussian (zero OAM) beam with all perturbative corrections included. The major benefit of this method is that it provides a closed-form analytical representation of the beam’s phasor, which is the complex function of the beam’s spatiotemporal amplitude and phase that satisfies the scalar Helmholtz equation [12,24]. This is a distinct advantage of the complex point-source model as compared to other methods [20–22], in which the fields are usually defined using either a series or an integral representation. The complex point-source model, however, still has one major drawback. Namely, the point-source Gaussian phasor solution is known to contain singularities

in its square modulus as well as a discontinuity at the beam waist [29].

The *complex source-sink* model [29] was developed to avoid the discontinuity and singularities encountered in the complex point-source model. The complex source-sink model represents the beam as two counter-propagating spherical waves, both centered at the imaginary location used in the complex point-source model. In this new model, the singularities and discontinuity in the square modulus of the Gaussian phasor both vanish.

In this paper, we show that the discontinuities still arise in phasors generated from the complex source-sink model for all odd OAM modes. The discontinuity in the phasor leads directly to discontinuities in the electromagnetic (EM) fields. Thus real fields generated from the complex source-sink phasor are nonphysical for odd OAM values.

This paper is organized as follows. In Sec. II, we discuss use of the phasor in determining the EM fields and highlight the source of their discontinuities. In Sec. III, we demonstrate analytically why the discontinuity appears in the phasor for odd OAM, and why it does not appear for even OAM. It is also shown how the discontinuity can be avoided. In Sec. IV, we present numerical results illustrating the discontinuities in electric-field components that result from the discontinuity in the phasor. In Sec. V, we summarize our results and present our conclusions.

II. PHASOR AND FIELD EQUATIONS

Traditionally, solving the full Helmholtz problem involves finding six field solutions to the vector Helmholtz equations. Matters are greatly simplified when instead one needs to find only a single solution to the scalar Helmholtz equation. This one solution is the beam’s phasor.

From a general expression for a phasor, Hertz potentials [30,31] (alternatively “Hertz vectors” or “polarization potentials”) can be used to generate exact expressions for the complex EM fields. The Hertz vectors, defined in Eq. (1) for a linearly polarized beam propagating in the \hat{z} direction, are represented in general as the complex phasor with a direction chosen based on the beam polarization:

$$\Pi_e = \psi(\mathbf{r}, t) \hat{\mathbf{x}}, \quad (1a)$$

$$\Pi_m = \eta_0 \psi(\mathbf{r}, t) \hat{\mathbf{y}}. \quad (1b)$$

Here, $\psi(\mathbf{r}, t)$ is the phasor and η_0 is the impedance of free space.

The Hertz potentials are sometimes referred to as “super-potentials” because they directly generate the usual scalar and vector EM potentials, which in turn generate the EM fields. Consequently, the complex vector fields \mathbf{E} and \mathbf{B} can be obtained directly from the Hertz potentials [30], and therefore from the phasor

$$\mathbf{E} = \nabla \times \nabla \times \Pi_e - \mu_0 \frac{\partial}{\partial t} (\nabla \times \Pi_m), \quad (2a)$$

$$\mathbf{H} = \nabla \times \nabla \times \Pi_m + \epsilon_0 \frac{\partial}{\partial t} (\nabla \times \Pi_e). \quad (2b)$$

Using the complex source-sink model, April [32,33] proposed an analytically exact discontinuity-free representation of the phasor for nonparaxial LG beams of any radial and OAM mode. April’s methods have since been adopted in many other works (e.g., [34–41]). As long as one considers only the square modulus of phasor solutions derived from the complex source-sink method, such as April’s phasor, the discontinuity and singularities are absent as claimed [33,42]. This does not mean, however, that the phasors themselves are discontinuity free. As we show in Sec. III, consideration of the real and/or imaginary parts of the source-sink phasor, depending on the choice of initial phase ϕ_0 , very clearly reveals a discontinuity at the beam waist for certain parameters. The presence of this axial discontinuity depends on the choice between two representations of the complex radius of curvature of the spherical waves, \tilde{R} [33,43].

Most work using April’s phasor (e.g., [34–37,39,41]) has so far been done with the lowest order LG mode (the “Gaussian mode,” which has zero OAM) or by considering the phasor only in the paraxial limit. As we will show, the phasors for these two common cases are not affected by this discontinuity.

III. DISCONTINUITY IN THE PHASOR

April [33] combined the complex source-sink method with use of a Poisson-like frequency spectrum [21,44], $f(\omega)$, to analytically represent the generic phasor $U_{p,n}$ from which EM fields can be derived using the Hertz potentials. For the zero order radial mode ($p = 0$), April’s phasor for the nonparaxial LG beam with any OAM index n can be expressed as [see Eqs. (16) and (17) of [33]]

$$U_{0,n}(\mathbf{r}, \omega) = \frac{4 \cos(n\phi)}{(2n-1)!!} f(\omega) \left(\frac{ka}{2}\right)^{1+n/2} \times \exp(-ka) P_n^n(\chi) j_n(k\tilde{R}), \quad (3)$$

where j_n is the spherical Bessel function, a is the confocal parameter of the focused beam, ϕ is the cylindrical angle, and the complex-valued associated Legendre function $P_n^n(\chi)$ is defined by Eqs. (8.6.6) and (8.6.18) of Ref. [45],

$$P_n^n(\chi) = (\chi^2 - 1)^{n/2} \frac{d^n}{d\chi^n} \left(\frac{1}{2^n n!} \frac{d^n(\chi^2 - 1)^n}{d\chi^n} \right), \quad (4)$$

in which the complex argument, χ , is defined by

$$\chi \equiv (z + ia)/\tilde{R}. \quad (5)$$

There are two choices [cf. Eq. (14) of Ref. [33]] for the complex spherical radius of curvature, \tilde{R} , in Eq. (3):

$$\tilde{R}_1 = \sqrt{\rho^2 + (z + ia)^2}, \quad (6a)$$

$$\tilde{R}_2 = i\sqrt{-\rho^2 - (z + ia)^2}, \quad (6b)$$

where ρ, ϕ, z are the cylindrical coordinates in which $\hat{\mathbf{z}}$ is the direction of propagation. The Poisson-like frequency spectrum $f(\omega)$ in Eq. (3) is defined as [see Eq. (4) of [21] or Eq. (20) of [33]]

$$f(\omega) = 2\pi e^{i\phi_0} \left(\frac{s}{\omega_0}\right)^{s+1} \frac{\omega^s \exp(-s\omega/\omega_0)}{\Gamma(s+1)} \theta(\omega), \quad (7)$$

where s is the spectral parameter [21,44] (which is related to the bandwidth of the pulse, which in turn is related to its duration), ω_0 is the frequency at which $f(\omega)$ has its maximum, ϕ_0 is the phase of the pulse, and $\theta(\omega)$ is the Heaviside unit step function.

It has been stated [33,43] that neither choice of \tilde{R} in Eq. (6) would cause the phasor to suffer from discontinuities, but we will show that only the choice \tilde{R}_2 produces continuous phasor components across the beam waist for all values of OAM.

Note also that the associated Legendre functions defined in Eq. (4) contain a branch cut only for odd index n . The following sections will elucidate the interplay between this branch cut and the choice of \tilde{R} , and show how this determines whether or not the phasors contain discontinuities.

A. Odd OAM modes

Inspection of Eqs. (3)–(7) shows that only the last two factors in the phasor may lead to the existence of a discontinuity. We thus focus on these two factors and express Eq. (3) as

$$U_{0,n}(\mathbf{r}, \omega) = c_n(\phi, \omega) P_n^n(\chi) j_n(k\tilde{R}), \quad (8)$$

where $c_n(\phi, \omega)$ is defined by comparison of Eqs. (3) and (8). To illustrate how the choice of \tilde{R} determines whether or not there is a discontinuity in the phasor, we consider the simplest odd OAM mode, $n = 1$. We first use the choice \tilde{R}_1 to demonstrate a discontinuity at the beam waist, $z = 0$.

1. Exact expansion of $U_{0,1}$ in powers of \tilde{R}

Expressing the spherical Bessel function in Eq. (8) in terms of sines and cosines [cf. Eqs. (A1)–(A3)] and defining the parameter

$$\xi \equiv k\tilde{R}, \quad (9)$$

the $n = 1$ phasor may be expressed as

$$U_{0,1} = c_1 P_1^1(\chi) \left(-\frac{\cos(\xi)}{\xi} + \frac{\sin(\xi)}{\xi^2} \right). \quad (10)$$

Replacing the trigonometric functions by their series expansions, we obtain

$$U_{0,1} = c_1 P_1^1(\chi) \left[-\frac{1}{\xi} \sum_{m=0}^{\infty} \frac{(-1)^m \xi^{2m}}{(2m)!} + \frac{1}{\xi^2} \sum_{m=0}^{\infty} \frac{(-1)^m \xi^{2m+1}}{(2m+1)!} \right]. \quad (11)$$

Combining the two summations, we obtain

$$U_{0,1} = c_1 P_1^1(\chi) \frac{1}{\xi} \sum_{m=0}^{\infty} \kappa_m \xi^{2m}, \quad (12a)$$

$$\kappa_m \equiv (-1)^{m+1} \frac{2m}{(2m+1)!}, \quad (12b)$$

where, from Eq. (4),

$$P_1^1(\chi) = \sqrt{\chi^2 - 1}. \quad (13)$$

2. $U_{0,1}$ with the choice $\tilde{R} = \tilde{R}_1$

Making the choice $\tilde{R} = \tilde{R}_1$ [defined in Eq. (6a)] in Eqs. (5) and (9), $U_{0,1}$ in Eq. (12a) becomes

$$U_{0,1} = \sqrt{\frac{-\rho^2}{\rho^2 + (z + ia)^2}} \frac{1}{\sqrt{\rho^2 + (z + ia)^2}} \times c_1 \sum_{m=0}^{\infty} (\kappa_m k^{2m-1}) (\rho^2 + (z + ia)^2)^m. \quad (14)$$

We see that the summation in Eq. (14) involves integer powers of complex numbers, whereas the prefactors multiplying the summation include two square roots of complex numbers, whose evaluation requires some care. In general, when dealing with products of square roots of complex numbers, it is best to evaluate each square root separately by expressing each complex number in terms of its magnitude and phase before taking its square root. In particular, multiplying the arguments of two square roots before taking the square root can lead to erroneous results. (For example, $\sqrt{-1} \times \sqrt{-1} = i \times i = -1$, but $\sqrt{-1 \times -1} = \sqrt{1} = 1$.) Thus we have expressed each of the complex arguments of the two square root prefactors in Eq. (14) in polar notation before taking the square roots. The result is

$$U_{0,1} = c_1 \exp\left(\frac{i}{2}(\phi_1 - \phi_2)\right) \sum_{m=0}^{\infty} \lambda_m \exp(im\phi_2), \quad (15a)$$

$$\phi_1 = \arctan\left(\frac{2az}{-\rho^2 + a^2 - z^2}\right), \quad (15b)$$

$$\phi_2 = \arctan\left(\frac{2az}{\rho^2 - a^2 + z^2}\right), \quad (15c)$$

$$\lambda_m \equiv (\kappa_m k^{2m-1}) \rho \times [(\rho^2 + z^2 + a^2)^2 - (2a\rho)^2]^{(m-1)/2}. \quad (15d)$$

Here, the real numbers λ_m are m -dependent magnitudes, defined in Eq. (15d), and ϕ_1 and ϕ_2 are the phases of the complex numbers inside the first and second square-root prefactors in Eq. (14) [which originate from $P_1^1(\chi)$ and \tilde{R}_1 , respectively]. The arctan function is defined over $-\pi < \phi \leq \pi$; thus arctan has a branch cut along the negative real axis. At the beam waist $z=0$, the imaginary parts of the complex numbers whose phases are given by ϕ_1 and ϕ_2 are zero; thus the branch cut along the negative real axis of each arctan function in Eqs. (15b) and (15c) is determined by the region over which the denominators in each of their arguments is negative. At

$z=0$ the denominator of ϕ_1 is negative for $\rho > a$, while that for ϕ_2 is negative for $\rho < a$.

The ϕ_1 and ϕ_2 phase factors multiplying the sum in Eq. (15a) always have a phase difference of π across the branch cut due to their overall factor of $1/2$ in the exponential. The key point is that ϕ_1 and ϕ_2 have branch cuts over different regions of the parameter ρ/a . Specifically, $U_{0,1}$ is discontinuous for $\rho > a$ at $z=0$ owing to the change in sign of $\phi_1/2$ across the branch cut, while for $\rho < a$ it is discontinuous owing to the change in sign of $\phi_2/2$ across the branch cut. Consequently, $U_{0,1}$ is discontinuous across the beam waist at $z=0$ for all values of ρ/a owing to the discontinuity in the product of phases, $\exp(\frac{i}{2}(\phi_1 - \phi_2))$. These ranges of the ratio ρ/a over which the discontinuities in the phases $\phi_1/2$, $-\phi_2/2$, and $(\phi_1 - \phi_2)/2$ occur are illustrated in the three panels of Fig. 1.

Note that, for each term in the sum in Eq. (15a), there is a phase factor involving an integer multiple of ϕ_2 . However, each of these terms is continuous across the branch cut since each branch contains an integer number m of full periods, resulting in a 2π phase difference across the branch cut. Thus the terms in the sum do not contribute to any discontinuity.

3. $U_{0,1}$ with the choice $\tilde{R} = \tilde{R}_2$

Use of the choice $\tilde{R} = \tilde{R}_2$ results instead in the phasor $U_{0,1}$ being continuous, as may be seen using the same arguments as in the previous section. Specifically, we replace \tilde{R}_1 by \tilde{R}_2 [defined in Eq. (6b)] in Eqs. (5) and (9) and substitute the results in Eq. (12a). Since $\tilde{R}_1^2 = \tilde{R}_2^2$, the terms in the summation are continuous across the branch cut. We thus focus on the new square root prefactors [corresponding to those for $\tilde{R} = \tilde{R}_1$ in Eq. (14)]:

$$U_{0,1} \propto \sqrt{\frac{-\rho^2}{\rho^2 + (z + ia)^2}} \frac{1}{\sqrt{-\rho^2 - (z + ia)^2}}. \quad (16)$$

The number inside the first square root factor is the same as in Eq. (14); consequently, it has the same phase factor, $\exp(i\phi_1)$. The number inside the square root in the denominator of the second factor in Eq. (16) has the phase factor $\exp(i\phi_3)$, where

$$\phi_3 = \arctan\left(\frac{-2az}{-\rho^2 + a^2 - z^2}\right). \quad (17)$$

Thus the phasor has the same form as in Eq. (15a), but with a different phase outside the sum, i.e.,

$$U_{0,1} = -ic_1 \exp\left(\frac{i}{2}(\phi_1 - \phi_3)\right) \sum_{m=0}^{\infty} \lambda_m \exp(im\phi_2). \quad (18)$$

By considering the branch cut in arctan, one can see that both ϕ_1 and ϕ_3 are discontinuous in the same region, namely for $\rho > a$. In both cases, the value changes sign as the $z=0$ plane is crossed. When these two phase factors are multiplied together as in Eq. (18), each one has a phase jump of π [cf. Figs. 1(a) and 2(a)], so that their product has a phase jump of 2π , as shown in Fig. 2(b). Hence the phasor defined by Eq. (18) is continuous across the branch cut.

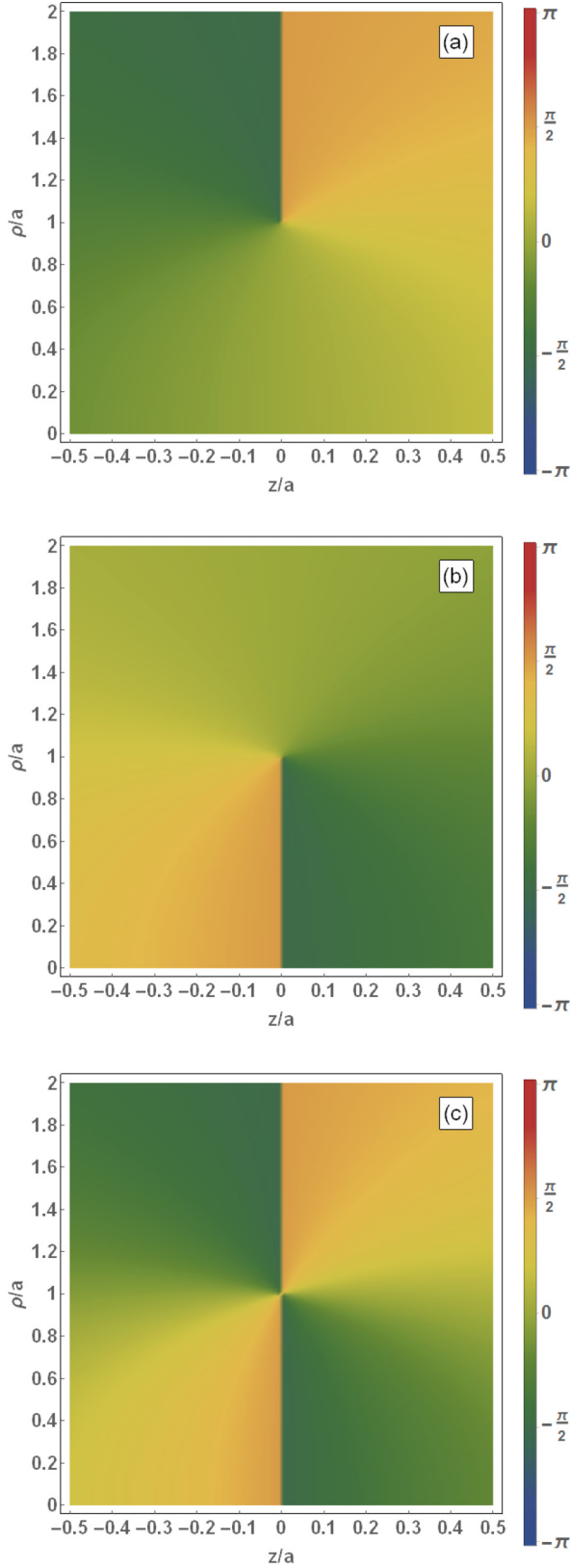


FIG. 1. Phases (a) $\phi_1/2$, (b) $-\phi_2/2$, and (c) $(\phi_1 - \phi_2)/2$ as functions of ρ/a and z/a , where a is the confocal parameter of the focused laser beam. Values of each phase over the range from $-\pi$ to $+\pi$ are indicated by the vertical color coding strip to the right of each panel. A phase jump of π occurs for $\rho/a > 1$ in (a), for $\rho/a < 1$ in (b), and for all values of ρ/a in (c). See text for discussion.

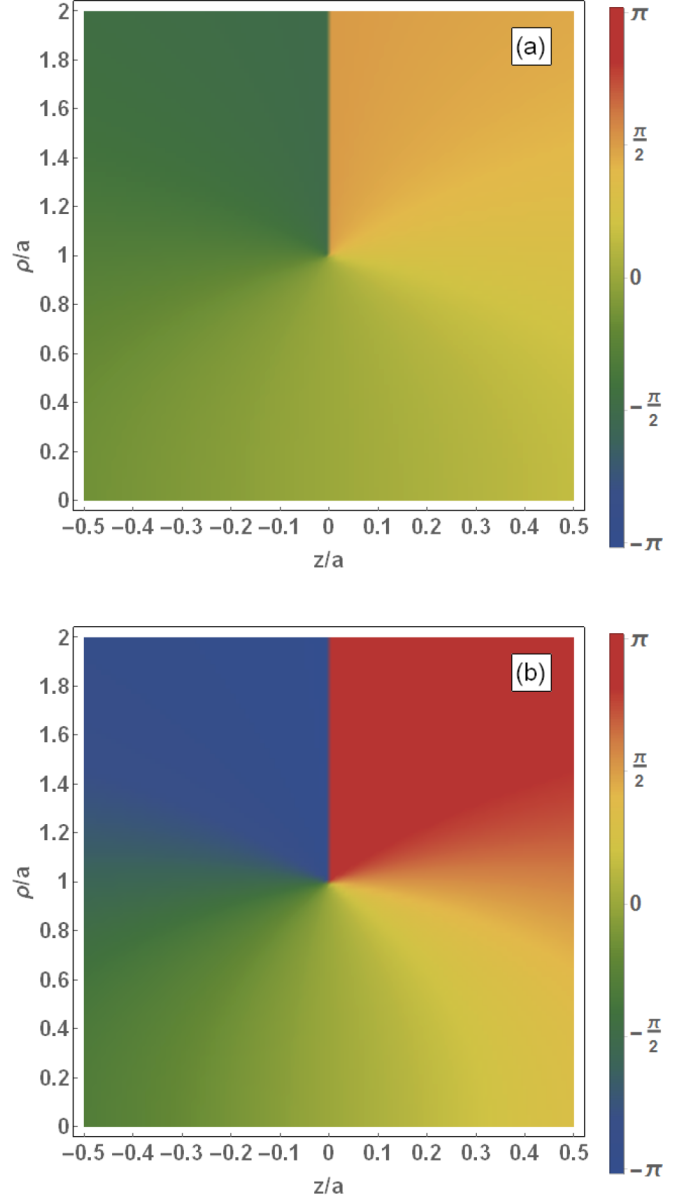


FIG. 2. Phases (a) $-\phi_3/2$ and (b) $(\phi_1 - \phi_3)/2$ as functions of ρ/a and z/a , where a is the confocal parameter of the focused laser beam and the behavior of the phase $\phi_1/2$ is shown in Fig. 1(a). Values of each phase over the range from $-\pi$ to $+\pi$ are indicated by the vertical color coding strip to the right of each panel. For $\rho/a > 1$ a phase jump of π occurs in (a) and a phase jump of 2π occurs in (b). See text for discussion.

4. Case of arbitrary odd OAM modes

We may easily see that for any odd OAM index n in Eq. (8), the phasor $U_{0,n}$ will exhibit the same behaviors as just shown for the $n = 1$ case. First, the associated Legendre function $P_n^n(\chi)$ in Eq. (4) always introduces a square root factor as on the right-hand side of Eq. (13) for any odd index n , which in turn results in the first square-root factor in Eqs. (14) and (16) regardless of whether one chooses respectively $\tilde{R} = \tilde{R}_1$ or $\tilde{R} = \tilde{R}_2$. Second, the spherical Bessel function factor j_n in Eq. (8) will always introduce the second square-root factor in Eqs. (14) and (16), depending respectively upon whether one

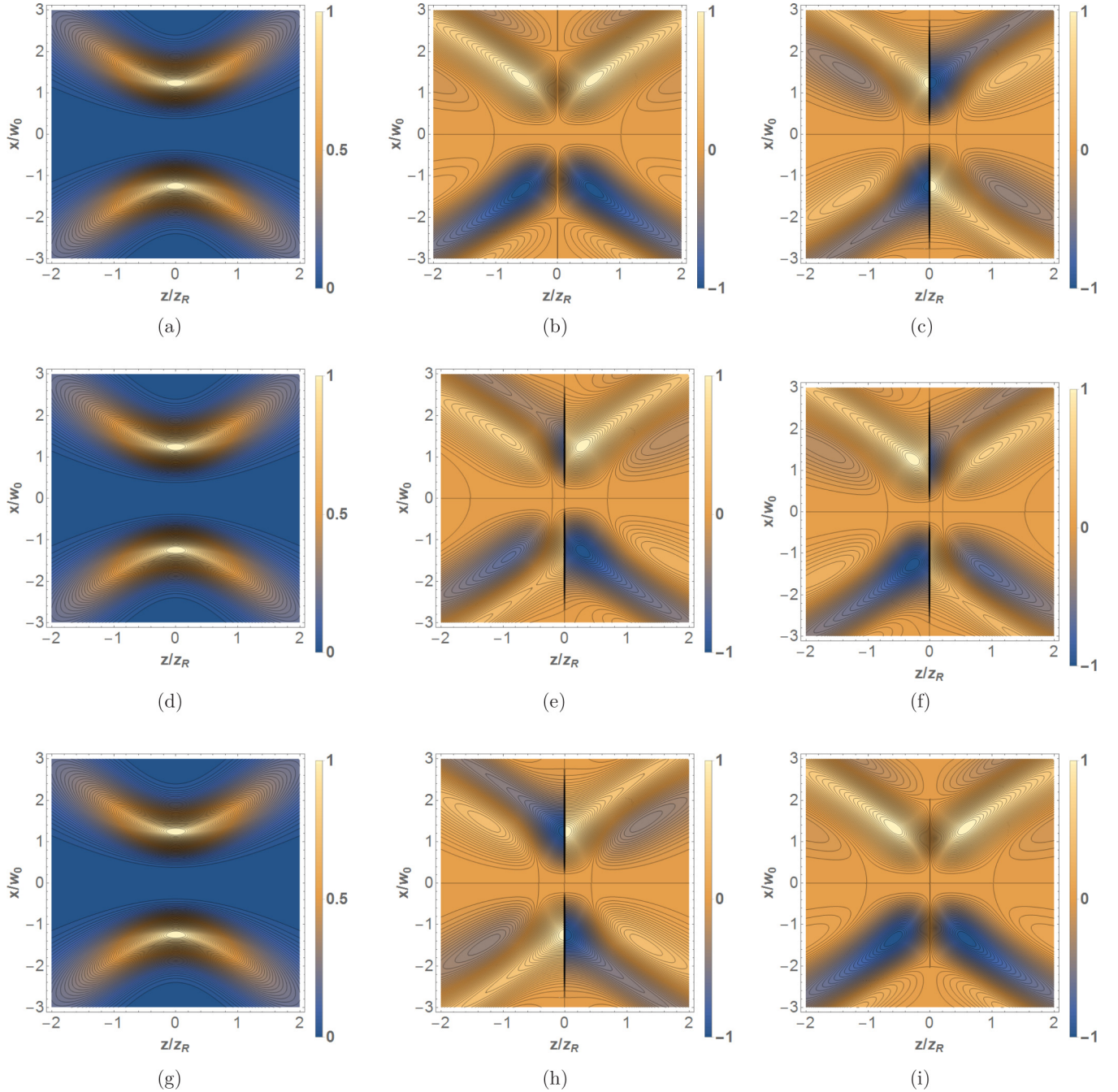


FIG. 3. Square modulus [(a),(d),(g)], real part [(b),(e),(h)], and imaginary part [(c),(f),(i)] of the phasor $U_{0,n}(\mathbf{r},t)$ in Eq. (19) for $n = 3$ for phases $\phi_0 = 0$ [(a)–(c)], $\phi_0 = \pi/4$ [(d),(e),(f)], and $\phi_0 = \pi/2$ [(g),(h),(i)]. Here, x, y, z are the Cartesian coordinates. The real and imaginary parts of the phasor are normalized to have a maximum amplitude of unity, and were calculated using the choice $\tilde{R} = \tilde{R}_1$ at $y = 0$ and $t = z/c$. The linearly polarized beam is assumed to have a spectral parameter $s = 712$, beam waist $w_0 = 2 \mu\text{m}$, wavelength $\lambda = 800 \text{ nm}$, and Rayleigh length $z_R \approx 15.7 \mu\text{m}$. See text for discussion.

chooses $\tilde{R} = \tilde{R}_1$ or $\tilde{R} = \tilde{R}_2$. One may see this by examining the expression for the spherical Bessel function given in Eq. (A1). Specifically, for odd n the square-root factor comes from the factor $1/\tilde{R}$ outside the square brackets in Eq. (A1); for odd n the two summations inside the square brackets in Eq. (A1) involve only even powers of \tilde{R} and hence do not contribute any square root factors. Thus the discontinuity in the phasor $U_{0,n}$ for a particular choice of \tilde{R} has the same behavior for any odd OAM n .

B. Even OAM modes

For even OAM modes n , the general expression for the phasor in Eq. (3) has the same form as in Eq. (8). As already been noted above, the associated Legendre function defined in Eq. (4) does not have a branch cut for even index n . We thus focus on the spherical Bessel function j_n in Eq. (8), using the expression for j_n in Eq. (A1). From Eqs. (A2) and (A3) we see that for any OAM mode n the functions P and Q involve respectively even and odd powers of \tilde{R} . For even

n , the sine and cosine functions in Eq. (A1) may be expanded respectively in terms of odd and even powers of \tilde{R} . Thus the two terms inside the square bracket in Eq. (A1) each involve odd powers of \tilde{R} . Owing to the $1/\tilde{R}$ factor multiplying the square bracket in Eq. (A1), the spherical Bessel function j_n for even n may thus be expressed as an expansion in even powers of \tilde{R} . Consequently, since $\tilde{R}_1^2 = \tilde{R}_2^2$ the spherical Bessel function j_n for even n is independent of the choice of the expression used for \tilde{R} . Also, since there are no odd powers of \tilde{R} in the expression for j_n for even n , no branch cuts are introduced. Thus the phasor $U_{0,n}$ for even n has no discontinuities.

IV. DISCONTINUITY IN THE REAL FIELDS

We can express the phasor of Eq. (3) in the time domain via a Fourier transformation,

$$U_{0,n}(\mathbf{r}, t) = \frac{1}{\sqrt{2\pi}} \int U_{0,n}(\mathbf{r}, \omega) \exp(i\omega t) d\omega, \quad (19)$$

the result of which is presented for arbitrary n in Eq. (A5) of Appendix A. Recall that the frequency spectrum $f(\omega)$ of the pulse, defined in Eq. (7), introduces an overall phase factor $\exp(i\phi_0)$ in both the frequency-dependent and time-dependent phasors in Eqs. (3) and (19), respectively. Therefore, changes in the initial phase ϕ_0 can affect the occurrence of discontinuities in the real and imaginary components of the phasor.

Figure 3 shows explicitly the discontinuities in the time domain phasor for $n = 3$ when using the choice $\tilde{R} = \tilde{R}_1$ for three values of the phase ϕ_0 . These plots were generated for a linearly polarized beam with spectral parameter $s = 712$, beam waist $w_0 = 2 \mu\text{m}$, wavelength $\lambda = 800 \text{ nm}$, and Rayleigh length $z_R = kw_0^2/2$. As expected, no discontinuity is visible in the square modulus of the time domain phasor for any ϕ_0 . However, the discontinuity at $z = 0$ is clearly visible in the real and/or imaginary parts of the phasor, depending upon the value of ϕ_0 [cf. panels (c), (e), (f), and (h) of Fig. 3].

In Fig. 4, we plot the longitudinal fields E_z [obtained using Eq. (2)] for the odd OAM phasors $U_{0,n}(\mathbf{r}, t)$ for $n = 1$ and $n = 3$ using the choice $\tilde{R} = \tilde{R}_1$ and an overall phase $\phi_0 = \pi$. This choice of the phase ϕ_0 yields a discontinuity in the imaginary parts of each of the phasors, which in turn results in discontinuous fields E_z . The corresponding transverse fields (not shown) are continuous across the beam waist at $z = 0$. In general, for linearly polarized fields, our calculations show that discontinuities in the real part of the time domain phasor lead to discontinuities in the transverse components of \mathbf{E} and \mathbf{B} , while discontinuities in the imaginary part of the time domain phasor lead to discontinuities in the longitudinal components of the fields. When both the real and imaginary parts of the phasor have discontinuities, the problem appears in all real field components.

As for the case of linear polarization, other beam polarizations will also suffer discontinuous real fields for phasors calculated using the choice $\tilde{R} = \tilde{R}_1$. These discontinuities originate in the phasor, which is polarization independent. The polarization only enters when computing the fields using the Hertz potentials, as Eq. (1) demonstrates for the case of linear polarization. The discontinuities may occur in different field

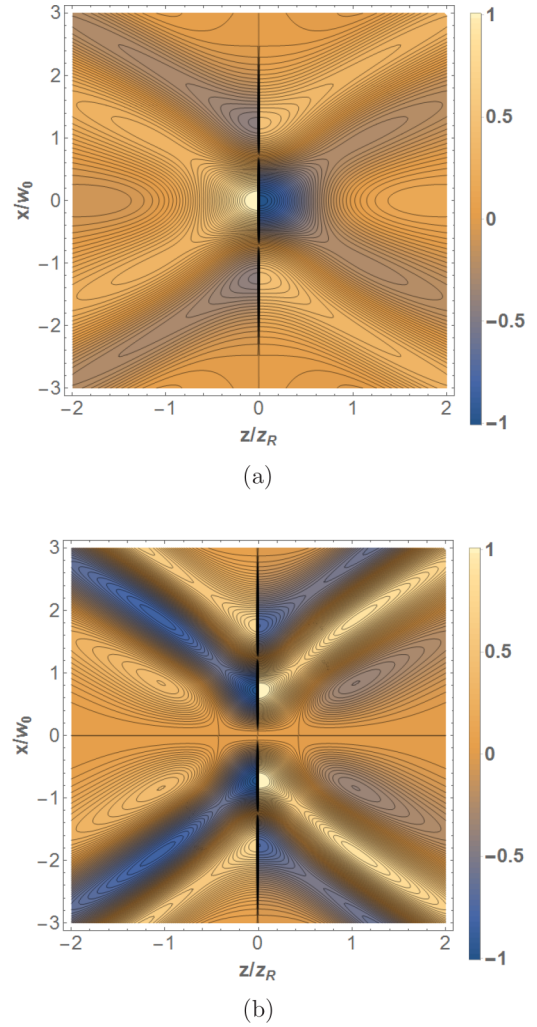


FIG. 4. Discontinuities in the longitudinal fields E_z [obtained using Eq. (2)] across the beam waist $z = 0$ for the odd OAM phasors $U_{0,n}$ for (a) $n = 1$ and (b) $n = 3$. These fields were obtained using the choice $\tilde{R} = \tilde{R}_1$ for a phase $\phi_0 = \pi$, $y = 0$, and $t = z/c$. The amplitudes of the fields are normalized to unity. See text for discussion.

components, depending on the field polarization, but they will be present in the real fields nonetheless.

Although our focus in this paper is on solutions to the nonparaxial Helmholtz equation, a brief mention of the paraxial case is warranted. In the paraxial limit of the phasor [cf. Eq. (5) of Ref. [33]], the terms $P_n^n(\chi)$ and \tilde{R} do not enter. In fact, to lowest radial order the associated Laguerre polynomials in the paraxial phasor are unity. Thus the real and imaginary parts of the paraxial phasor, by direct inspection, are simple oscillatory functions of z . In this limit, therefore, the problem of discontinuities in the fields does not arise.

V. SUMMARY AND CONCLUSIONS

In this work, we have shown (by examining the nonparaxial source-sink phasor) that for all odd OAM modes discontinuities arise across the entire beam waist when the choice $\tilde{R} = \tilde{R}_1$ is made for the complex spherical radius. Whether these discontinuities lie in the real or imaginary parts of the phasor depends upon the overall phase ϕ_0 of the laser pulse. In

turn, these phasor discontinuities result in nonphysical real electromagnetic field components calculated from the Hertz potentials.

As we have shown, these problems do not exist for even OAM modes. Further, in the paraxial limit, the terms that cause discontinuous behavior are not present in the phasor expression. Thus real components of paraxial fields are free from discontinuities in the phasor that cause problems in the nonparaxial case.

Whether considering the fields of vortex beams in vacuum, or interacting with plasmas or other media, proper physical theoretical models are necessary. As this work has shown, discontinuities in the nonparaxial source-sink phasor can be avoided completely by making the choice $\tilde{R} = \tilde{R}_2$ for the complex spherical radius. Such a choice avoids discontinuities in the complex phasor for all OAM modes.

ACKNOWLEDGMENTS

We gratefully acknowledge informative discussions with Alexandre April regarding his work. Computational results were obtained using facilities at the Holland Computing Center of the University of Nebraska-Lincoln. This work was supported in part by the U.S. Department of Energy, Office of Science, Basic Energy Sciences, under Grant No. DE-FG02-96ER14646, and by the U.S. Air Force Office of Scientific Research under Award No. FA9550-14-1-0345 (A.F.S.).

APPENDIX: EXPLICIT EXPRESSION FOR THE PHASOR $U_{0,n}(\mathbf{r}, t)$

In this appendix we present the result of carrying out the Fourier transform of the phasor $U_{0,n}(\mathbf{r}, \omega)$ in Eq. (3), which is obtained from Eqs. (16) and (17) of Ref. [33] for the phasor $\tilde{U}_{0,n}^\sigma(\mathbf{r}, \omega)$ upon setting $\sigma = e$ and $p = 0$ (and dropping the explicit notation of the parity $\sigma = e$ in our calculations). In order to carry out the Fourier transform in Eq. (19), one must expand the spherical Bessel function in Eq. (3) using Eq. (10.1.8) of Ref. [45]:

$$j_n(k\tilde{R}) = \frac{1}{k\tilde{R}} \left[P\left(n + \frac{1}{2}, k\tilde{R}\right) \sin\left(k\tilde{R} - \frac{n\pi}{2}\right) + Q\left(n + \frac{1}{2}, k\tilde{R}\right) \cos\left(k\tilde{R} - \frac{n\pi}{2}\right) \right], \quad (\text{A1})$$

where

$$P\left(n + \frac{1}{2}, k\tilde{R}\right) = \sum_{m=0}^{\lfloor n/2 \rfloor} (-1)^m (2k\tilde{R})^{-(2m)} \frac{(n+2m)!}{(2m)! \Gamma(n-2m+1)} \quad (\text{A2})$$

and

$$Q\left(n + \frac{1}{2}, k\tilde{R}\right) = \sum_{m=0}^{\lfloor (n-1)/2 \rfloor} (-1)^m (2k\tilde{R})^{-(2m-1)} \times \frac{(n+2m+1)!}{(2m+1)! \Gamma(n-2m)}. \quad (\text{A3})$$

1. Result for $U_{0,n}(\mathbf{r}, t)$

Expanding the trigonometric functions in Eq. (A1) in terms of exponentials and replacing k everywhere by $k = \omega/c$, one

may carry out the Fourier transform in Eq. (19) by making repeated use of the integral representation of the gamma function [cf. Eq. (6.1.1) of [45]], i.e.,

$$\Gamma(\gamma + 1) = \eta^{\gamma+1} \int_0^\infty d\omega \omega^\gamma \exp(-\eta\omega), \quad \text{Re } \eta > 0. \quad (\text{A4})$$

The result for $U_{0,n}(\mathbf{r}, t)$ is

$$U_{0,n}(\mathbf{r}, t) = C_n \cos(n\phi) P_n^n(\chi) \left\{ \sum_{m=0}^{\lfloor n/2 \rfloor} A(n, m) \left(\frac{c}{\tilde{R}}\right)^{2m+1} \times [(T_-)^{-(s+n/2-2m+1)} - (-1)^n (T_+)^{-(s+n/2-2m+1)}] + \sum_{m=0}^{\lfloor (n-1)/2 \rfloor} D(n, m) \left(\frac{c}{\tilde{R}}\right)^{2m+2} [(T_-)^{-(s+n/2-2m)} + (-1)^n (T_+)^{-(s+n/2-2m)}] \right\}. \quad (\text{A5})$$

In Eq. (A5) we have defined

$$A(n, m) \equiv \frac{i(-1)^{m+1}(n+2m)!}{(2m)! \Gamma(n-2m+1)} \times \frac{\Gamma(s+n/2-2m+1)}{2^{(2m+1)} \Gamma(s+1)} \left(\frac{s}{\omega_0}\right)^{(2m-n/2)}, \quad (\text{A6})$$

$$D(n, m) \equiv \frac{(-1)^m (n+2m+1)!}{(2m+1)! \Gamma(n-2m)} \times \frac{\Gamma(s+n/2-2m)}{2^{(2m+2)} \Gamma(s+1)} \left(\frac{s}{\omega_0}\right)^{(2m+1-n/2)}, \quad (\text{A7})$$

where s and ω_0 are defined in the text below Eq. (7),

$$C_n \equiv \exp[i(\phi_0 - n\pi/2)] \left(\frac{a}{c}\right)^{(1+n/2)} \frac{2^{(1-n/2)}}{(2n-1)!!} \quad (\text{A8})$$

and

$$T_\pm \equiv 1 - \frac{i\omega_0 t}{s} + \frac{a\omega_0}{cs} \pm \frac{i\omega_0 \tilde{R}}{cs}. \quad (\text{A9})$$

2. Result for $U_{0,1}(\mathbf{r}, t)$

Setting $n = 1$ in Eq. (A5), we have

$$C_1 = \exp[i(\phi_0 - \pi/2)] \sqrt{2} \left(\frac{a}{c}\right)^{3/2}, \quad (\text{A10})$$

$$A(1, 0) = -i \frac{\Gamma(s+3/2)}{2\Gamma(s+1)} \left(\frac{s}{\omega_0}\right)^{-1/2}, \quad (\text{A11})$$

$$D(1, 0) = \frac{\Gamma(s+1/2)}{2\Gamma(s+1)} \left(\frac{s}{\omega_0}\right)^{1/2}. \quad (\text{A12})$$

Hence

$$U_{0,1}(\mathbf{r}, t) = C_1 \cos(\phi) P_1^1(\chi) \left\{ A(1, 0) \left(\frac{c}{\tilde{R}}\right) [(T_-)^{-(s+3/2)} + (T_+)^{-(s+3/2)}] + D(1, 0) \left(\frac{c}{\tilde{R}}\right)^2 [(T_-)^{-(s+1/2)} - (T_+)^{-(s+1/2)}] \right\}. \quad (\text{A13})$$

- [1] G. A. Mourou, T. Tajima, and S. V. Bulanov, Optics in the relativistic regime, *Rev. Mod. Phys.* **78**, 309 (2006).
- [2] A. Di Piazza, C. Müller, K. Z. Hatsagortsyan, and C. H. Keitel, Extremely high-intensity laser interactions with fundamental quantum systems, *Rev. Mod. Phys.* **84**, 1177 (2012).
- [3] M. Lax, W. H. Louisell, and W. B. McKnight, From Maxwell to paraxial wave optics, *Phys. Rev. A* **11**, 1365 (1975).
- [4] J. P. Barton and D. R. Alexander, Fifth-order corrected electromagnetic field components for a fundamental Gaussian beam, *J. Appl. Phys.* **66**, 2800 (1989).
- [5] S. M. Sepke and D. P. Umstadter, Exact analytical solution for the vector electromagnetic field of Gaussian, flattened Gaussian, and annular Gaussian laser modes, *Opt. Lett.* **31**, 1447 (2006).
- [6] S. M. Sepke and D. P. Umstadter, Analytical solutions for the electromagnetic fields of tightly focused laser beams of arbitrary pulse length, *Opt. Lett.* **31**, 2589 (2006).
- [7] S. X. Hu and A. F. Starace, Laser acceleration of electrons to giga-electron-volt energies using highly charged ions, *Phys. Rev. E* **73**, 066502 (2006).
- [8] Y. I. Salamin, Fields of a Gaussian beam beyond the paraxial approximation, *Appl. Phys. B* **86**, 319 (2007).
- [9] L.-W. Pi, S. X. Hu, and A. F. Starace, Favorable target positions for intense laser acceleration of electrons in hydrogen-like, highly-charged ions, *Phys. Plasmas* **22**, 093111 (2015).
- [10] *Twisted Photons*, edited by J. P. Torres and L. Torner (Wiley-VCH, New York, 2011).
- [11] A. M. Yao and M. J. Padgett, Orbital angular momentum: Origins, behavior and applications, *Adv. Opt. Photon.* **3**, 161 (2011).
- [12] *The Angular Momentum of Light*, edited by D. L. Andrews and M. Babiker (Cambridge University Press, Cambridge, UK, 2013).
- [13] M. Zürch, C. Kern, P. Hansinger, A. Dreischuh, and C. Spielmann, Strong-field physics with singular light beams, *Nat. Phys.* **8**, 743 (2012).
- [14] C. Hernández-García, A. Picón, J. San Román, and L. Plaja, Attosecond Extreme Ultraviolet Vortices from High-Order Harmonic Generation, *Phys. Rev. Lett.* **111**, 083602 (2013).
- [15] G. Gariepy, J. Leach, K. T. Kim, T. J. Hammond, E. Frumker, R. W. Boyd, and P. B. Corkum, Creating High-Harmonic Beams with Controlled Orbital Angular Momentum, *Phys. Rev. Lett.* **113**, 153901 (2014).
- [16] V. E. Lembessis, M. Babiker, and D. Ellinas, *The Role of Gouy Phase on the Mechanical Effects of Laguerre-Gaussian Light Interacting with Atoms*, AIP Conf. Proc. No. 1742 (AIP, Melville, NY, 2016), p. 030009.
- [17] M. Vaziri, M. Golshani, S. Sohaily, and A. Bahrapour, Electron acceleration by linearly polarized twisted laser pulse with narrow divergence, *Phys. Plasmas* **22**, 033118 (2015).
- [18] G. Molina-Terriza, J. P. Torres, and L. Torner, Twisted photons, *Nat. Phys.* **3**, 305 (2007).
- [19] Q. Xiao, C. Klitis, S. Li, Y. Chen, X. Cai, M. Sorel, and S. Yu, Generation of photonic orbital angular momentum superposition states using vortex beam emitters with superimposed gratings, *Opt. Express* **24**, 3168 (2016).
- [20] B. Richards and E. Wolf, Electromagnetic diffraction in optical systems. II. Structure of the image field in an aplanatic system, *Proc. R. Soc. A* **253**, 358 (1959).
- [21] C. F. R. Caron and R. M. Potvliege, Free-space propagation of ultrashort pulses: Space-time couplings in Gaussian pulse beams, *J. Mod. Opt.* **46**, 1881 (1999).
- [22] M. A. Bandres and J. C. Gutiérrez-Vega, Higher-order complex source for elegant Laguerre-Gaussian waves, *Opt. Lett.* **29**, 2213 (2004).
- [23] Q. Lin, J. Zheng, and W. Becker, Subcycle Pulsed Focused Vector Beams, *Phys. Rev. Lett.* **97**, 253902 (2006).
- [24] A. E. Siegman, *Lasers* (University Science Books, New York, 1986).
- [25] G. A. Deschamps, Gaussian beam as a bundle of complex rays, *Electron. Lett.* **7**, 684 (1971).
- [26] S. Y. Shin and L. B. Felsen, Gaussian beam modes by multipoles with complex source points, *J. Opt. Soc. Am.* **67**, 699 (1977).
- [27] A. L. Cullen and P. K. Yu, Complex source-point theory of the electromagnetic open resonator, *Proc. R. Soc. A* **366**, 155 (1979).
- [28] M. Couture and P.-A. Belanger, From Gaussian beam to complex-source-point spherical wave, *Phys. Rev. A* **24**, 355 (1981).
- [29] Z. Ulanowski and I. K. Ludlow, Scalar field of nonparaxial Gaussian beams, *Opt. Lett.* **25**, 1792 (2000).
- [30] J. A. Stratton, *Electromagnetic Theory* (McGraw-Hill, New York, 1941).
- [31] J. D. Jackson, *Classical Electrodynamics* (Wiley, New York, 1995).
- [32] A. April, Nonparaxial elegant Laguerre-Gaussian beams, *Opt. Lett.* **33**, 1392 (2008).
- [33] A. April, Ultrashort, strongly focused laser pulses in free space, in *Coherence and Ultrashort Pulse Laser Emission*, edited by F. J. Duarte (InTech, New York, 2010), Chap. 16, p. 355.
- [34] V. Marceau, A. April, and M. Piché, Electron acceleration driven by ultrashort and nonparaxial radially polarized laser pulses, *Opt. Lett.* **37**, 2442 (2012).
- [35] X. Chu, Evolution of elegant Laguerre-Gaussian beam disturbed by an opaque obstacle, *J. Electromagn. Waves Appl.* **26**, 1749 (2012).
- [36] V. Marceau, C. Varin, T. Brabec, and M. Piché, Femtosecond 240-keV Electron Pulses from Direct Laser Acceleration in a Low-Density Gas, *Phys. Rev. Lett.* **111**, 224801 (2013).
- [37] A. Sell and F. X. Kärtner, Attosecond electron bunches accelerated and compressed by radially polarized laser pulses and soft-x-ray pulses from optical undulators, *J. Phys. B: At., Mol., Opt. Phys.* **47**, 015601 (2014).
- [38] F. Fillion-Gourdeau, C. Lefebvre, and S. MacLean, Scheme for the detection of mixing processes in vacuum, *Phys. Rev. A* **91**, 031801 (2015).
- [39] V. Marceau, P. Hogan-Lamarre, T. Brabec, M. Piché, and C. Varin, Tunable high-repetition-rate femtosecond few-hundred keV electron source, *J. Phys. B: At., Mol., Opt. Phys.* **48**, 45601 (2015).
- [40] L. J. Wong, B. Freelon, T. Rohwer, N. Gedik, and S. G. Johnson, All-optical three-dimensional electron pulse compression, *New J. Phys.* **17**, 013051 (2015).
- [41] C. Varin, V. Marceau, P. Hogan-Lamarre, T. Fennel, M. Piché, and T. Brabec, MeV femtosecond electron pulses from direct-field acceleration in low density atomic gases, *J. Phys. B: At., Mol., Opt. Phys.* **49**, 024001 (2016).

- [42] C. J. R. Sheppard and S. Saghafi, Beam modes beyond the paraxial approximation: A scalar treatment, *Phys. Rev. A* **57**, 2971 (1998).
- [43] C. J. R. Sheppard, High-aperture beams: Reply to comment, *J. Opt. Soc. Am. A* **24**, 1211 (2007).
- [44] S. Feng and H. G. Winful, Spatiotemporal structure of isodiffracting ultrashort electromagnetic pulses, *Phys. Rev. E* **61**, 862 (2000).
- [45] *Handbook of Mathematical Functions*, edited by M. Abramowitz and I. A. Stegun (National Bureau of Standards, Gaithersburg, MD, 1972).